

**EMMLi: A maximum likelihood approach to the analysis of modularity**

Journal:	<i>Evolution</i>
Manuscript ID	Draft
Manuscript Type:	Brief Communication
Date Submitted by the Author:	n/a
Complete List of Authors:	Goswami, Anjali; University College London, Genetics, Evolution & Environment Finarelli, John; University College Dublin, School of Biology & Environmental Science
Keywords:	Morphological Evolution, phenotypic integration, trait correlations, mammals, model selection

1 EMMLi: A maximum likelihood approach to the analysis of modularity

2 Running Header: Maximum likelihood analysis of modularity

3

4 Anjali Goswami<sup>1</sup> and John A. Finarelli<sup>2,3</sup>

5

6 <sup>1</sup>Department of Genetics, Evolution & Environment and Department of Earth Sciences,

7 University College London, London, WC1E 6BT, UK

8 <sup>2</sup>School of Biology & Environment Science, University College Dublin, Science Centre – West,

9 Belfield, Dublin 4, Ireland.

10 <sup>3</sup>UCD Earth Institute, University of College Dublin, Belfield, Dublin 4, Ireland.

11 Emails: a.goswami@ucl.ac.uk; john.finarelli@ucd.ie

12

13 Keywords: phenotypic integration, trait correlations, mammals, model selection

14

15 **ABSTRACT**

16 Identification of phenotypic modules, semi-autonomous sets of highly-correlated traits, can be  
17 accomplished through exploratory (e.g., cluster analysis) or confirmatory approaches (e.g., RV  
18 coefficient analysis). While statistically more robust, confirmatory approaches are generally  
19 unable to compare across different model structures. For example, RV coefficient analysis finds  
20 support for both two- and six-module models for the therian mammalian skull. Here, we present  
21 a maximum likelihood approach that takes into account model parameterization. We compare  
22 model log-likelihoods of trait correlation matrices using the finite-sample corrected Akaike  
23 Information Criterion, allowing for comparison of hypotheses across different model structures.  
24 Simulations varying model complexity and within- and between-module contrast demonstrate  
25 that this method correctly identifies model structure and parameters across a wide range of  
26 conditions. We further analyzed a dataset of 3-D data, consisting of 61 landmarks from 181  
27 macaque (*Macaca fuscata*) skulls, distributed among five age categories, testing 31 models,  
28 including no modularity among the landmarks, and various partitions of 2, 3, 6, and 8 modules.  
29 Our results clearly support a complex six-module model, with separate within- and inter-module  
30 correlations. Furthermore, this model was selected for all five age categories, demonstrating that  
31 this complex pattern of integration in the macaque skull appears early and is highly conserved  
32 throughout postnatal ontogeny. Subsampling analyses demonstrate that this method is robust to  
33 relatively low sample sizes, as is commonly encountered in rare or extinct taxa. This new  
34 approach allows for the direct comparison of models with different parameterizations, providing  
35 an important tool for the analysis of modularity across diverse systems.

36

37 **INTRODUCTION**

38 The related topics of phenotypic integration and modularity, which concern associations among  
39 traits and their partitioning into semi-autonomous and highly-correlated subsets, respectively,  
40 have received increased attention over the past few decades as a powerful bridge among different  
41 scales of evolutionary analysis. Recent years have seen increasing effort to identify and compare  
42 phenotypic modularity and integration across taxa, in some cases spanning entire vertebrate  
43 ‘classes’ (Goswami 2006b, a; Goswami 2007; Porto et al. 2009; Bell et al. 2011; Bennett and  
44 Goswami 2011; Klingenberg and Marugan-Lobon 2013), and even comparing plants and animals  
45 (Conner et al. 2014). There has also been a refining of different levels of modularity acting at  
46 different scales. The most typically-studied level, termed “variational” (Marquez 2008) or  
47 “static” (Klingenberg 2014) modularity, focuses on a single species or population, commonly at  
48 a specific ontogenetic stage (e.g., adults). Within this level, analyses focus on identifying drivers  
49 of trait integration, whether functional, developmental, genetic, or environmental. Beyond  
50 variational modularity, studies have analyzed modularity at the ontogenetic scale (that is,  
51 patterns or changes in modularity through ontogeny within a species), and evolutionary  
52 modularity (comparative analysis of patterns of modularity across taxa). Coincident with this  
53 increase in studies of modularity, there has been an explosion in the number of methods  
54 proposed to analyze phenotypic modularity and integration, both within and across populations  
55 (Klingenberg 2009; Goswami and Polly 2010; Klingenberg 2013; Adams and Felice 2014;  
56 Bookstein and Mitteroecker 2014; Klingenberg 2014).

57

58 Analyses of modularity have taken many forms, from entirely exploratory approaches, such as  
59 cluster analysis, Euclidean distance matrix analysis, and graphical modelling, to confirmatory  
60 approaches, such as partial least squares analysis and the related RV coefficient analysis,  
61 integration matrices, and theoretical matrix modelling (reviewed in Klingenberg 2009; Goswami  
62 and Polly 2010; Klingenberg 2013, 2014), and there has been a vigorous discussion of the merits,  
63 practical considerations, and issues of each approach (Klingenberg 2008; Goswami and Polly  
64 2010; Fruciano et al. 2013; Adams and Felice 2014). Not surprisingly, confirmatory methods are  
65 generally viewed as more robust, particularly as exploratory methods such as cluster analysis  
66 impose hierarchical relationships on traits that may or may not reflect their true biological  
67 organization. On the other hand, exploratory approaches have the benefit of not requiring *a*  
68 *priori* determination of model structure, whereas confirmatory methods depend on a defined  
69 model structure and are therefore limited to testing pre-selected models. Given the complexity of  
70 many biological structures, and the diverse factors that may influence trait relationships  
71 (Hallgrímsson et al. 2009), this limitation argues for the continued role of exploratory  
72 approaches, particularly as studies expand beyond well-established model systems. Recent work  
73 has developed relative eigenanalysis for the purpose of comparing two covariance matrices in a  
74 more informative manner than do previous methods, such as eigenvalue dispersion or random  
75 skewers analysis (Bookstein and Mitteroecker 2014), providing an efficient exploratory approach  
76 that can detail the specific ways that high-dimensional covariance matrices differ by identifying  
77 the maximal ratios of variance between any two groups. However, this approach does not  
78 directly address the problem of describing the pattern of integration for a group, which remains  
79 an outstanding issue in this field.

80

81 Another important issue with most current confirmatory approaches is that they are designed to  
82 measure support for alternative hypothesized parameter values within a proposed model structure  
83 (Wagner 2000). For example, RV coefficient analysis determines the correlations among sets of  
84 traits, and then randomizes trait associations to produce an empirical distribution of RV  
85 coefficients for the model structure under consideration, testing the hypothesis that the observed  
86 RV coefficient is significantly lower than randomized alternatives. But while this methodology  
87 can test if a particular model is more structured than random, it does not readily address the  
88 question of whether a four-module model describes the pattern of phenotypic integration better  
89 than arrangements with three or five modules. The same is true of the recently described  
90 Covariance Ratio metric (Adams 2016), which improves upon several statistical issues with RV  
91 coefficient analysis, but also can only test one model of modularity against a hypothesis of  
92 random associations of traits. Thus far, only one published method allows for comparisons of  
93 models with different complexities (Marquez 2008), as demonstrated with a 2-D landmark  
94 dataset for rodent mandibles. This method included several innovations that allowed for testing  
95 of hundreds of alternative models, including those with overlapping landmarks, but the most  
96 relevant is the correction of similarity among the observed and modeled covariance matrices  
97 against the number of estimated parameters. This addition facilitates comparison across models  
98 with varying structures of different complexity. While this represented an important step in  
99 confirmatory tests of modularity, the author noted that a linear correction for the number of  
100 estimated parameters may not be appropriate for all test statistics or for more complex  
101 approaches (Marquez 2008). Additionally, this method has also never been expanded to 3-D  
102 data.

103

104 Here, we describe a new method for the analysis of phenotypic modularity from trait correlation  
 105 matrices based on a maximum likelihood approach. We provide a case study applying this  
 106 approach to a dataset of macaque skulls spanning infant to adult age groups. We use this method  
 107 to compare various models that have been proposed for mammalian skull modularity (including  
 108 no modularity, a two-module neurocranial/facial hypothesis, and multiple six-module  
 109 hypotheses; Fig. 1), as well as novel alternative models of varying structure and complexity.

110

### 111 *EMMLi: Evaluating Modularity with Maximum Likelihood*

112 Model selection approaches using information theory compare likelihood fits across a set of  
 113 models of varying degree of complexity. In order to estimate likelihoods of models of trait  
 114 integrations, we first model the expected distribution around a hypothesized value representing  
 115 the relationship among a set of traits. For the product moment correlation coefficient, and its  
 116 derivatives including the congruence coefficient and canonical correlation (Goswami and Polly  
 117 2010), a simple transformation is available in the Fisher r-to-z transformation:

118

$$119 \text{ Eq. 1) } z_r = \mathbf{tanh}^{-1}(r) = \frac{1}{2} \ln \left( \frac{1+r}{1-r} \right) \text{ (Sokal and Rohlf 1995, pg. 575),}$$

120

121 where  $r$  is the sample correlation coefficient. Here the observed correlation matrix is treated as a  
 122 set of realizations (the values of  $r$ ) of a hypothesized true correlation coefficient ( $\rho$ ). The

123 distribution around a hypothesized value of  $\rho$  is approximately normally distributed with  
 124 parameters:

125

126 Eq. 2a)  $\mu_\rho = z_\rho = \frac{1}{2} \ln \left( \frac{1+\rho}{1-\rho} \right)$  and ,

127 Eq. 2b)  $\sigma_\rho^2 = \left( \frac{1}{\sqrt{n-3}} \right)^2 = \frac{1}{n-3}$  (Sokal and Rohlf 1995, page 575),

128

129 where  $n$  is the sample size used to calculate the correlation coefficient (i.e., the number of  
 130 specimens with measured landmarks). The log-likelihood support for a hypothesized value of  $\rho$ ,  
 131 given an observed value of  $r$ , is then:

132

133 Eq. 3)  $\text{LogL} \propto -\frac{1}{2} \text{Ln}(\sigma_\rho^2) - \frac{(z_r - \mu_\rho)^2}{2\sigma_\rho^2}$  (Edwards 1992).

134

135 Applying Equation 3 to a matrix of trait correlations, the simplest model structure (no  
 136 modularity) proposes a single value for the correlation coefficient between all possible trait pairs.  
 137 The value that maximizes the summed log-likelihood for all observed correlations in the matrix  
 138 would then be the preferred hypothesis, and this log-likelihood would then be the model log-  
 139 likelihood for the “no modularity” model structure.

140



141 However, given the results of a large number of previous studies (Cheverud 1982, 1989, 1995a,  
 142 1996; Ackermann and Cheverud 2000; Marroig and Cheverud 2001; Hallgrimsson et al. 2004;  
 143 Goswami 2006a; Hallgrimsson et al. 2009; Porto et al. 2009; Goswami and Polly 2010;  
 144 Klingenberg 2013), it is highly likely that a model structure positing a single value of  $\rho$  for the  
 145 entire correlation matrix would not adequately describe trait correlations in a real biological  
 146 system. Model structures of varying complexity can be compared using the Akaike Information  
 147 Criterion (AIC) (Akaike 1973; Burnham and Anderson 2002), assessing the likelihood fit of the  
 148 models, while controlling for better fit induced by increased model complexity. The finite-  
 149 sample AIC ( $AIC_c$ ) is given by:

150

151 Eq. 4)  $AIC_c = -2\text{Log}L + 2K + \frac{2K(K+1)}{N-K-1}$  (Hurvich and Tsai 1989).

152

153 In Equation 4,  $N$  is the sample size, but in the case of computing  $AIC_c$ , this is the number of  
 154 between-trait correlations used to calculate the likelihood score.  $K$  is the number of estimated  
 155 parameters, which is the number of distinct, optimal correlations estimated by the model, and an  
 156 additional parameter for each estimate of the variance around the hypothetical value of  $\rho$  (see:  
 157 Equation 2b). In the present analysis, this is fixed for all of the examined models within each  
 158 data set (a single variance was calculated for each data set based on its sample size), and the  
 159 number of parameters is simply the number of estimated values of  $\rho$  incremented by one for all  
 160 models. However, this does not need to be the case, as more complex analyses may wish to  
 161 consider whether patterns of modularity are common across multiple data sets which may have

162 different estimates of variance. In such cases, different variances may be included as estimated  
163 parameters among different models.

164

165 To illustrate the designation of model parameters more clearly, consider a set of landmarks  
166 across a mammal cranium (Fig. 2A). Previous study of the mammal skull has proposed six  
167 modules for this system (Cheverud 1982; Goswami 2006a). It is possible that that the  
168 magnitudes of within-module correlations are effectively the same in all of the modules (Fig. 2B)  
169 or that each of these modules has distinct strengths of correlation between landmarks within a  
170 given module (Fig. 2C). Furthermore, inter-module correlations could also be distinct for each  
171 module-to-module set (Fig. 2E and G), or they could be effectively identical (Fig. 2D and F).

172 These variations then returns four potential model structures with 3, 17, 8 or 22 estimated  
173 parameters (the number of estimated  $\rho$ 's in each, plus 1 for the estimated variance). Summing the  
174 log-likelihoods from Equation 3 for the set of observed correlations within each modeled set for  
175 an optimal estimate of  $\rho$ , gives the model log-likelihood. These can be compared to one another,  
176 to the “no modularity” hypothesis, and to different proposed structures or different groupings of  
177 the landmarks within modules using Equation 4. From the model  $AIC_c$  scores, we calculate  
178  $\Delta AIC_c$ , the difference between a particular model's  $AIC_c$  score and the lowest score observed  
179 among the tested models. From this, we calculate the model log-likelihood adjusting for the  
180 penalty due to parameterization:

181

182 Eq. 5) **Model LogL**  $\propto -\frac{1}{2}\Delta AIC_c$  (Burnham and Anderson 2002).

183

184 A set of model posterior probabilities can then be calculated by dividing each model's likelihood  
185 by the sum of likelihoods over the set of examined models (N.B. these are likelihoods, and are  
186 therefore equal to  $e^{\text{Model LogL}}$  (see: Burnham and Anderson 2004)).

187

### 188 *A Note on Sample Size*

189 A value of "n" or sample size appears in both the equations for calculating the variance around  
190 an estimated value of  $\rho$  (Equation 2b) and for the calculation of the AIC statistic (Equation 5).

191 We have used upper- and lowercase to distinguish between the two, as  $n$  for calculation of  
192 correlations is based on the number of specimens, whereas, in the case of computing  $AIC_c$ ,  $N$  is  
193 the number of between-trait correlations considered in calculating the log-likelihood. For a 61  
194 landmark data matrix, there are 1830 unique between-landmark correlations (i.e., the sub-  
195 diagonal values of the matrix).

196

### 197 *A note on the use of the Fisher Transformation*

198 The Fisher r-to-z Transformation converts the bounded correlation coefficient to an unbounded  
199 variable. Comparison of the transformed correlation to a hypothetical population value of  $\rho$   
200 demonstrates that the transformed coefficient is approximately normally distributed about  $\rho$ ,  
201 making the Fisher Transformation attractive for hypothesis testing. In the case of the correlation  
202 matrix, however, there is a concern about the independence of the sample of correlation

203 coefficients, in that, for example, elements  $r_{12}$  and  $r_{13}$  are not strictly random *iid* draws from a  
204 population, but are themselves intercorrelated. However, the Fisher-transformed correlations  
205 within a correlation matrix have been shown to be asymptotically, multivariate normal in  
206 distribution, and robust to the violations of independence (Steiger 1980b; De Leeuw 1983).  
207 Specifically, this has been demonstrated for pattern hypotheses within correlation matrices,  
208 wherein observed correlation coefficients are tested against a proposed “pattern matrix” (Steiger  
209 1980a), and this approach, which is adopted here in the form of the proposed within- and among-  
210 module correlation estimates, has been applied in a wide range of research questions (Feldman et  
211 al. 2007; Wager et al. 2007; LeBel and Gawronski 2009). As such the employing Fisher-  
212 transformed correlations in a likelihood framework, as proposed here, should prove a reliable  
213 approach to evaluating modularity with trait correlation matrices.

214

## 215 **SIMULATIONS**

216 Given the above noted concern with respect to independence of the Fisher-transformed  
217 correlation coefficients, we evaluated the ability of the maximum likelihood approach as  
218 implemented in EMLLi to correctly select a known model when choosing among models  
219 structures. To do so, we conducted an extensive series of simulations testing a range of model  
220 structures, contrasting two variables: model complexity (number of parameters) and contrast  
221 (difference between within-module and between-module strength of integration). In all cases, 60  
222 “landmarks” were simulated as divided into zero, two or six modules, to represent a hypothetical  
223 correlation structure that we wish to evaluate. Between-module correlations were set at a mean  
224 value of 0.1 for all simulations. Standard deviations for generating correlations were varied from

225 a low value of  $\sigma = 0.01$  to realistic value of  $\sigma = 0.05$  (e.g., Cheverud 1982), encompassing values  
226 used in simulations testing other recently described methods for the analysis of modularity  
227 (Adams 2016).

228

229 Simulating datasets without any modular structure allowed for assessment of Type I error rates.  
230 100 permutations each were run with the mean correlations among all traits simulated as  $r =$   
231 0.15, 0.3, 0.5, 0.7, or 0.9, with  $\sigma = 0.01$  or 0.05, for a total of 1000 simulations. In these cases,  
232 the correct model would be equivalent in structure to model 1 (K=2) in Table 1.

233

234 For the two and six module structures, both simple and complex models were tested. The simple  
235 models involved two or six modules which all had the same within-module correlations, set to  
236 five mean values ranging from  $r = 0.15$  in the lowest contrast model to  $r = 0.9$  in the highest  
237 contrast model (i.e., mean within-module  $r = 0.15, 0.3, 0.5, 0.7,$  and  $0.9$  were all simulated).

238

239 For the complex models, all two or six modules had different within-module correlations. In the  
240 high contrast, complex two-module model, these values were set to mean within-module  $r = 0.7$   
241 and  $0.9$ ; in the mix contrast model, mean within-module  $r = 0.3$  and  $0.8$ ; and in the low contrast  
242 case, mean within-module  $r = 0.15$  and  $0.3$ . In the high contrast, complex six-module model,  
243 mean within-module  $r = 0.7, 0.75, 0.8, 0.85, 0.9,$  and  $0.95$ ; in the mix contrast case, mean within-  
244 module  $r = 0.3, 0.4, 0.5, 0.6, 0.7,$  and  $0.8$ ; and in the low contrast case, mean within-module  $r =$   
245  $0.15, 0.2, 0.25, 0.3, 0.35,$  and  $0.4$ . For the simple two-module structure, the correct model would

246 be equivalent in structure to model 2 ( $K=3$ ) in Table 1, and the complex structure would be  
247 equivalent to model 3 ( $K=4$ ). For the simple six-module structure, the correct model would be  
248 equivalent in structure to model 4 or 8 ( $K=3$ ) in Table 1, and the complex structure would be  
249 equivalent to model 5 or 9 ( $K=8$ ). 100 permutations each of these 16 models were run, using  
250 each of the standard deviation levels, resulting in 3200 total simulations of these modular  
251 structures.

252

253

## 254 **CASE STUDY: MAXIMUM LIKELIHOOD ANALYSIS OF MACAQUE CRANIAL** 255 **MODULARITY**

### 256 *Materials*

257 We use a data set of 3-D coordinates for 61 landmarks taken on the cranium of Japanese  
258 macaque (*Macaca fuscata*) from the Primate Research Institute at Inuyama, Japan, previously  
259 described in (Goswami and Polly 2010) (see Supporting Information). Individuals were divided  
260 into five datasets representing four age classes: infants with deciduous dentition only ( $n = 42$ ),  
261 juveniles with M1 erupted ( $n = 42$ ), sub-adult with M2 erupted ( $n = 48$ ), and adults with the  
262 entire adult dentition, further divided into male and female data partitions ( $n_m = 25$ ,  $n_f = 24$ ). See  
263 Goswami and Polly (2010) for further details on the dataset used in the following analyses.

264

265 The landmark data were superimposed with Generalized Procrustes superimposition to remove  
266 the effects of rotation, translation and size (scaling all specimens to unit centroid size). All five  
267 datasets were analyzed separately. We calculated vector congruence coefficient correlation  
268 matrices, producing 61x61 element matrices. This vector-based approach allows for  
269 simultaneous analysis of all three coordinates representing a single landmark (Goswami 2006a;  
270 Goswami and Polly 2010). There has been some debate about the use of vector-based versus  
271 coordinate-based correlations in studies of phenotypic integration and modularity (Klingenberg  
272 2008; Goswami and Polly 2010; Klingenberg 2013). Here, we use the vector-based matrices, as  
273 we feel these better reflects biological relationships, treating each landmark as a single unit of  
274 information. However, we also include an example using the correlation matrix for individual  
275 coordinates for the M1-erupted data set (see Supporting Information). This is a 183x183 matrix  
276 (x-, y- and z-coordinates for each of 61 landmarks). Allometric effects and asymmetric variation  
277 have not been removed from the example dataset, for comparability with previously published  
278 analyses of macaque skull modularity (Cheverud 1982; Goswami and Polly 2010), although, as  
279 with selection of metric of trait correlation, the model presented here is applicable to datasets that  
280 do remove, or focus entirely on, those aspects of shape.

281

## 282 *Models*

283 We investigated 31 model structures within several broad hypotheses of cranial modularity. The  
284 first, and simplest, model structure is that there are no distinct modules within the cranium, and  
285 that the cranium can be analyzed as a single entity. Further, more complex, models of modularity  
286 consist of a two-module (neurocranial vs. facial) structure (Drake and Klingenberg 2010), two

287 six-module structures (primate-specific (Cheverud 1995b) and general mammalian (Goswami  
288 2006a)), and an eight-module structure combining the two six-module models (see: Table S1).  
289 We investigated further refinements for both configurations of the six-module structure: first,  
290 leaving some landmarks “unintegrated”, i.e., outside of any module, based on a monotreme  
291 model of integration (Goswami 2006a), resulting in 3-module + “unintegrated” models; and,  
292 second, considering a tissue-origin model (Goswami 2006a), in which landmarks were grouped  
293 based on their derivation from neural crest, mesodermal, or mixed germ-layer derived bone (see:  
294 Table S1).

295

296 As detailed above, each hypothesized model structure may have many potential  
297 parametrizations, depending on whether within-module or across-module correlations are  
298 modeled as being the same for all cases (e.g., a single high hypothesized correlation within  
299 modules and a single, across-module correlation), or all module cases are considered unique, or  
300 some mixture of these extremes. For example, the 2-module neurocranial/facial model structure  
301 comprises Models 2 and 3 (Table 1), with the difference being the number of proposed within-  
302 module estimates. Models with increasing numbers of modules have correspondingly greater  
303 complexity in their potential parameterizations. As described above, the six-module model has  
304 four different parameterizations examined here (Fig. 2). In the simplest model (Model 4, Fig.  
305 2D), there is a single within-module estimate and a single across-module estimate. Other models  
306 propose six freely-varying within-module estimates with a constant across-module estimate  
307 (Model 5, Fig. 2F), fifteen freely-varying across-module estimates with a single within-module  
308 estimate (Model 6, Fig 2E) and a completely varying model with six within-module estimates  
309 and 15 across-module estimates (Model 7, Fig. 2G). All model structures that were explored and



310 their corresponding parameterizations are given in Table 1. The R code used in this analysis and  
311 example data files are provided in the online supporting information for this article and are  
312 available for download from: <http://www.goswamilab.com/#!/software/c1cxq>.

313

#### 314 *Subsampling analysis*

315 While analyses of integration are often performed on model systems with the ability to sample  
316 large numbers of individuals, questions about the evolution of integration can require the  
317 incorporation of fossil or rare taxa (Goswami et al. 2015) for which sample sizes are constrained.  
318 To evaluate potential sensitivity of this method to small sample sizes, we conducted a  
319 subsampling analysis of the best sampled dataset (subadult *Macaca*, 48 specimens), producing  
320 50 random subsets each of 25 specimens, 15 specimens, and 10 specimens. Each subset was  
321 subjected to generalized Procrustes analysis prior to calculation of vector congruence coefficient  
322 correlation matrices, producing 61x61 element matrices and analyzed in EMMLi.

323

## 324 **RESULTS**

### 325 *Simulations*

326 When a low standard deviation ( $\sigma = 0.01$ ) around the simulated correlation values was used, the  
327 correct model structure was identified as the best fit model in 100% of cases for all no-module,  
328 two-module, and six-module structures (Fig. 3A). Reconstructed  $\rho$  values were consistently  
329 within 0.01 of the simulated values. For the simulations of a no-modularity data set, posterior

330 probabilities were generally low,  $\sim 0.24$ , even for the best fit model. All posterior probabilities  
331 for the correct model were greater than 0.5 for the simulations in which there was a modular  
332 structure to the data. In all cases, estimated  $p$  values exactly matched those used to generate the  
333 simulated datasets.

334

335 When a higher standard deviation of 0.05 was used, the correct model was identified in most  
336 cases, although accuracy decreased at the highest levels of mean correlations for simple  
337 structures (Fig. 3B). The correct model was selected with high ( $>0.90$ ) posterior probability in  
338 100% of cases for the simple six-module model with within-module correlations ranging from  
339 0.15 to 0.70. It was also correct, with 100% posterior probability, in all cases for the complex  
340 six-module structure, using either high, mixed, or low correlations. When all within-module  
341 correlations were set to 0.90, the correct model was selected in 23/100 runs, and receives a  
342 posterior probability  $> 0.05$  in 36/100 runs, with a different parameterization of the same model  
343 structure (six modules,  $K=8$ ) selected in all remaining cases. For the two-module model, the  
344 correct model was selected in 100% of cases for within-module correlations of 0.15, 0.30, and  
345 0.50. The correct model is selected in 84/100 cases when the within-module correlation is 0.7,  
346 and receives a posterior probability  $> 0.05$  in 100% of cases. In the remaining 16 runs, the  
347 closely related, more parameterized two-model model ( $K=3$ ) was selected as the best fit model.  
348 When within-module correlations are centered around 0.90, an unrelated model was selected in  
349 the majority of cases. The correct model was selected in 100% of cases with the complex two-  
350 module model using low or mixed correlations. When only the highest correlations (0.70 and  
351 0.90) were used to simulate a complex two-module structure, the correct model was selected in  
352 77/100 cases and had a posterior probability  $> 0.05$  in 83/100 cases.

353

354 The strongest effects of high correlations and higher standard deviation were observed in cases  
355 of no modularity in the simulated structure (Fig. 3B). The correct model was selected in 100%  
356 of cases when the overall correlation was 0.15 or 0.30. When the overall correlation was 0.50,  
357 the correct model was selected as the best fit model in 98/100 runs and had a posterior  
358 probability  $> 0.05$  in all runs. With overall correlations of 0.70, the correct model was selected  
359 as the best fit model in 53/100 cases and had a posterior probability  $> 0.05$  in 95 cases. In the  
360 cases where the wrong model was selected, the posterior probability was  $< 0.50$  in all but five  
361 cases, although, as noted above, posterior probabilities are generally low ( $\sim 0.2$ ) for models of no  
362 modularity, even when the correct model was selected. When the overall correlation was  
363 extremely high, 0.90, the wrong model was selected with posterior probability  $> 0.50$  in all runs.  
364 Even in cases where the wrong model was supported, estimated  $\rho$  values were within 0.03 of the  
365 values used to simulate each dataset.

366

### 367 *Case study*

368 For all five data sets, the optimal model selected by  $AIC_c$  was Model 7 (Fig. 1C), with over 99%  
369 of the posterior probability centered on this model for each data set, with the remaining model  
370 posterior probabilities were effectively zero for all other models considered (Tables 2, S2-S5).  
371 Additionally, the 183x183 raw coordinate data the juvenile (M1 erupted) data set (Table S6) also  
372 returned Model 7 as the unambiguously best-supported model. Model 7 can thus be considered  
373 the single optimal model describing the pattern of cranial integration in the macaque data set  
374 (Edwards 1992; Royall 1997; Burnham and Anderson 2002).

375

376 Model 7 is based on Cheverud's primate-specific six-module structure (Cheverud 1982),  
377 proposing distinct within-module  $\rho$ 's for all six modules, as well as separate  $\rho$ 's for all possible  
378 across-module comparisons (total of 22 estimated parameters). Model 16, for the adult female  
379 data set only, had a posterior probability of  $\sim 0.001$  (Table S2). This model is a variant of Model  
380 7, in which the oral, nasal, and occipital modules are maintained, but all other landmarks are  
381 treated as unintegrated, which is broadly similar to the pattern of modularity displayed by  
382 monotremes (Goswami 2006a). All other model structures, including those that proposed no  
383 modularity, a neurocranial/facial module structure, more than six cranial modules, or non-  
384 primate specific module structures, received no support.

385

386 Estimated values for  $\rho$  were similar for each of the 21 model parameters across the four data sets  
387 (Table 3), with very strongly integrated anterior modules (Modules 1 and 2, corresponding to the  
388 anterior dentition and nasal/facial bones) and a moderately integrated occipital region (Module  
389 6). Other modules, corresponding to the basicranium, neurocranium, and palatal/molar region  
390 were less well integrated, as were inter-module correlations. This is in approximate agreement  
391 with previous analyses of integration patterns in mammalian crania (Goswami 2006a).

392

### 393 *Subsampling analysis*

394 For the subsampling analyses, the unambiguously best supported model (posterior probabilities  $>$   
395 0.95) was the same as for the full dataset (Model 7) 100% of the time, for the rarefaction to 25

396 specimens. With 15 specimens, the same model was selected in 48/50 analyses. In the two cases  
397 of mismatch, Model 7 was one of three top models (posterior probability  $> 0.05$ ), sharing support  
398 with alternative parameterizations of the same Cheverud six-module structure. Subsampling to  
399 10 specimens recovered Model 7 in 36/50 of runs. In three of the remaining runs in which it  
400 wasn't the best fit model, it was selected as one of the top models ( $>0.05$  posterior probability),  
401 in all cases along with alternative parameterizations of the Cheverud six-module structure. For  
402 11 runs, Model 7 had a posterior probability less than 0.05. Thus, even at  $n=10$ , this method was  
403 successful at identifying the correct model as having a significant posterior probability 78% of  
404 the time. Moreover, of the 14 cases where Model 7 was not the top model, the best supported  
405 model was a variation on the Cheverud model in 12 cases. In only 2 of the 50 runs was the top  
406 model unrelated to Model 7; thus, a relevant model structure, if not the correct parameterization,  
407 was recovered in 96% of cases at  $n=10$ .

408

409 Reconstructed  $\rho$  values were consistently very similar to those of the full dataset (Table 4), even  
410 at  $n=10$ , with mean deviations from  $\rho$  values for the full dataset of 0.020 for  $n = 25$ , to 0.037 for  
411  $n = 15$ , and 0.062 for  $n = 10$ . Standard deviations of reconstructed  $\rho$  values were similarly low,  
412 but unsurprisingly increasing with decreasing sample sizes: 0.023 for  $n = 25$ , 0.036 for  $n = 15$ ,  
413 and 0.042 for  $n = 10$ . Thus, these further analyses provide strong support that this method is  
414 remarkably robust to quite low sample sizes.

415

416

417

418 **DISCUSSION**

419 Extensive simulations varying model complexity, magnitude of mean within-module correlation,  
420 and standard deviation of correlations demonstrates that this method is robust under biologically  
421 realistic conditions. It performs exceedingly well (perfectly, in fact), when correlations are  
422 tightly grouped around hypothetical values of  $\rho$  (low standard deviation simulations), regardless  
423 of whether the simulated structure is highly modular or entirely lacks any modular structure.  
424 With increased dispersion around the  $\rho$  values (higher standard deviations), this method is robust  
425 under most conditions, but struggles with highly integrated structures, specifically those that  
426 combine two biologically unlikely situations: 1) complete lack of modularity and 2) uniformly  
427 and, in most cases, unrealistically high correlations. Only in the case of very high within-module  
428 correlations (mainly  $\rho = 0.90$ , but also involving  $\rho = 0.70$  in the no-modularity model and in the  
429 high-correlation complex two-module model) does the method return incorrect model structures  
430 with high posterior probability. Observing such high correlations, uniformly across all modules  
431 or an entire structure is unusual. Previous studies (Conner et al. 2014) have shown that  
432 vertebrates, plants, and hemimetabolous insects display mean phenotypic correlations among  
433 linear traits ranging from 0.35 to 0.5, although mean correlations among linear traits in  
434 holometabolous insects may be much higher ( $\sim 0.84$ ). In the case study presented here, only a  
435 single module (Module 2) shows mean within-module correlations above 0.7 (Table 3), while all  
436 other modules are in the moderate to low range of within-module correlations used in these  
437 simulations. Our simulations also show that this method is extremely robust in identifying  
438 complex models of modularity in which some modules have high within-module correlations and  
439 others have moderate or low within-module correlations. Thus, outside of the unusual conditions

440 noted above, our method proves to work with high efficacy, and the few cases of “failure” in  
441 conditions typically encountered in most biological systems involved selection of a differently  
442 parameterized version of the same model structure.

443

444 We further note that no other method currently available for confirmatory analysis of modularity  
445 directly compares models of modularity against a model of total integration (e.g., Marquez 2008;  
446 Klingenberg 2009; Adams 2016). For example, in the description of the covariance ratio metric,  
447 the author provided the important cautionary note that covariance ratio analysis be used only for  
448 evaluating patterns of modularity and suggested that Partial Least Squares analysis (Rohlf and  
449 Corti 2000; Adams and Felice 2014) be used to evaluate hypotheses of integration (Adams  
450 2016). EMMLi thus provides unprecedented ability to evaluate models of total integration as  
451 well as models of modularity, but struggles with correctly identifying the lack of modularity  
452 when both standard deviations of correlations and mean correlations are high. For this reason,  
453 we urge caution in interpreting results if the returned posterior probabilities of the best fit models  
454 are low ( $< 0.50$ ), if reconstructed correlations are exceptionally high (uniformly  $> 0.70$ ), or if  
455 multiple unrelated models are returned with posterior probability  $> 0.05$ , particularly if standard  
456 deviations of within-module correlations are high. Under those circumstances, we follow Adams  
457 (2016) in suggesting that it may prove useful to employ Partial Least Squares analysis to  
458 evaluate the support for a highly integrated structure. We further advise users to consider and  
459 report all models with posterior probabilities greater than 0.05.

460

461 With regard to the macaque case study, for all five data sets, greater than 99% of the posterior  
462 probability distribution was explained by Model 7, the most parameterized version of  
463 Cheverud's model of six cranial modules. This result indicates very strong support for this model  
464 of cranial modularity in macaques. Cheverud's (1982) model structure was based on analysis of  
465 correlations among inter-landmark distances (length measurements) from a dataset of 462 rhesus  
466 macaques (*Macaca mulatta*). Cheverud (1982) identified support for this model by calculating an  
467 agreement statistic between the hypothesized F-sets and empirical P-sets, the latter derived by  
468 cluster analysis of inter-landmark distances in principal component space. This model structure  
469 has subsequently tested using theoretical matrix correlation analysis and RV coefficient analysis,  
470 with the present Japanese macaque dataset (*M. fuscata*) (Goswami and Polly 2010). However,  
471 that study also tested two alternative models: the two-module facial/neurocranial model (Models  
472 2-3 in Table 1), and an alternative six-module structure (the "Goswami" models, Models 8-11 in  
473 Table 1), based on general patterns of integration among therian mammals (Goswami 2006a). In  
474 that study, model selection was not directly possible, as RV coefficient analysis makes no  
475 specific hypothesis regarding model parameterization beyond the total number of modules and  
476 theoretical matrix correlation analysis simply compares the correspondence between two  
477 matrices, usually with a permutation test to assess support. All three model structures were  
478 supported at  $p < 0.01$  using theoretical matrix correlation analysis with Mantel's test, although it  
479 should be noted that Cheverud's model showed the highest correlations with the empirical data.  
480 In the RV coefficient analyses, the two-module model was supported in three of the five datasets  
481 ( $p < 0.05$ ), the Goswami model was supported in two of five datasets, and the Cheverud model  
482 supported in three of the five datasets, and, where supported, the Cheverud model received the



483 strongest support ( $p < 0.001$ ). However, it was not supported for either adult dataset, whereas  
484 both the two-module and the Goswami models received support for the adult male dataset.

485

486 The Goswami and Polly (2010) analysis highlighted an important issue with the existing range of  
487 confirmatory approaches to analyzing modularity: the lack of a clear way to compare among  
488 models across proposing fundamentally different structures of modularity/integration. One can  
489 compare the Cheverud six-module model to the Goswami six-module model with RV coefficient  
490 analysis, as they both are based on six cranial modules, yet neither can be meaningfully  
491 compared to the two-module neurocranial/facial model (Fig. 1). Moreover, there are a range of  
492 possibilities, from unintegrated traits within a partially modular structure, to entirely different  
493 modular structures that are biologically interesting and potentially informative, but which are  
494 impossible to approach with the existing methods.

495

496 The results presented demonstrate the unambiguous support for Cheverud's structure of  
497 phenotypic modularity for the macaque cranium, with distinct within- and among-model  
498 correlation values. Here, we used maximum likelihood analysis of congruence coefficients  
499 derived from multidimensional vector variables, as well as the more standard individual  
500 coordinate correlations for one dataset. We focused on trait correlation matrices, rather than  
501 variance-covariance matrices, in this method, as the relationships among traits, and not their  
502 individual variances, are the primary concern in studies of phenotypic integration and modularity  
503 (Olson and Miller 1951; Olson and Miller 1958; Pavlicev et al. 2009; Goswami and Polly 2010;  
504 Conner et al. 2014). Benefits of the model selection approach employed here include: 1) ability

505 to directly compare models of different complexities (such as two- and six-module models) or  
506 models of similar complexity which do not constitute nested subsets of one another (such as the  
507 Cheverud (1982) and Goswami (2006a) six-module models), 2) increased precision in model  
508 description, in terms of varying numbers of within- and between-module values for  $\rho$ ; and 3)  
509 expansion to mixed models, in which a structure can include both modules and unintegrated  
510 traits (e.g., models 20-31 in Table 1).

511

512 As noted above, there is an existing method to compare competing models of variational  
513 modularity using subspace analysis (Marquez 2008). As with the maximum likelihood approach  
514 described here, subspace analysis is a remarkably flexible approach that accurately reflects the  
515 complexity of biological systems and is capable of comparing hundreds of models (and indeed  
516 performs better with more models).

517

518 Both subspace analysis and EMMLi can test multiple variations on a basic model structure,  
519 allow for combined or overlapping modules, and conduct direct comparison of models with  
520 similar or different parametrizations. In contrast to maximum likelihood analysis as implemented  
521 in EMMLi, subspace analysis creates a specific hypothetical covariance matrix for each matrix  
522 that fixes between-module covariances at zero. This is rarely the case in biological systems,  
523 particularly in proximal modules, and therefore oversimplifies the apparent hierarchical pattern  
524 of modularity in systems such as the cranium. The maximum likelihood-based approach  
525 described here could be considered preferable because it does not assign an *a priori* value to  
526 between-module correlations, and by returning all estimated  $\rho$  values for the best supported

527 model(s), allows for direct assessment of every within- and between-module correlation, which  
528 can inform on alternative model structures to test (for example, if two modules show a between-  
529 module  $\rho$  that is equal or similar to their respective within-module  $\rho$  values, one could add an  
530 additional model that unites those modules into a single grouping).

531

532 The two methods also differ on the method of model selection. As a measure of goodness of fit  
533 between the observed and model covariance matrices, subspace analysis as implemented in  
534 MINT (Marquez 2008) uses  $\gamma$ , and corrects for differences in the parametrizations of each model  
535 by regressing  $\gamma$  against the number of zero elements in each model, generating  $\gamma^*$ , with  
536 significance evaluated against expectations from random covariance matrices. In order to  
537 strengthen the evaluation of model rank, a jackknifing approach was used, with model support  
538 reflecting how often a model ranked first in the jackknifed samples. The method described here  
539 does not require fixing any values, but instead provides an overall model structure and searches  
540 for values of  $\rho$  that return the maximum likelihood for that structure. The complexity of the  
541 model, and correction for the goodness of fit or model selection, is a function of the number of  
542 independent estimates of  $\rho$ , rather than the number of zero elements in the model.

543

544 Because subspace analysis as implemented in MINT has never been developed for 3-D data, we  
545 did not conduct a direct comparison of these two methods. Qualitative comparison of the  
546 simulations of subspace analysis (Marquez 2008) and those described here suggest that the  
547 maximum likelihood approach is more robust to sample size, number of models, model  
548 complexity, and magnitude of integration, as well as being available for use with any

549 morphometric dataset. Nonetheless, subspace analysis represented a major improvement on  
550 existing methods, and there are numerous interesting aspects to subspace analysis as  
551 implemented in MINT, such as the heuristic modeling of additional hypotheses of modularity  
552 and the construction of consensus models, both of which could be developed as exploratory tools  
553 within a likelihood framework.

554

555 In addition to the possibility of incorporating aspects of the Marquez (2008) method, which was  
556 developed for the same purpose as the maximum likelihood method described here, there is also  
557 vast potential for combining with methods developed for different goals. For example, the  
558 Reimmanian spaces for covariance matrices and the distances therein provide a framework for  
559 comparing the relative likelihood of one covariance matrix to that of another (Bookstein and  
560 Mitteroecker 2014) and could be combined with the method we describe here. In whatever  
561 combination, all of these methods are beginning to fill an important need for approaches that are  
562 more flexible to the biological reality of complex anatomy.

563

564 These benefits are important, as many studies of phenotypic modularity to date have either  
565 assumed a hypothesized set of modules without explicitly testing its validity for the taxon of  
566 interest (e.g., applying the Cheverud model to other mammals, as in Marroig et al. 2009; Porto  
567 et al. 2009), or have tested a single model in the absence of comparison to other potential  
568 models, regardless of the support for that one model (e.g., Klingenberg and Marugan-Lobon  
569 2013). Ongoing analyses of other groups suggest that the Cheverud model does not adequately  
570 describe all mammalian taxa. For example, EMMLi analysis of a 55 landmark data set for the red

571 fox, *Vulpes vulpes* (Table S7) recovered the 22-parameter version of the Goswami six-module  
572 model as the unambiguous best fit model (for details of dataset, see Goswami 2006b). This result  
573 is perhaps unsurprising, as that model was initially based on cluster analyses of a comparative  
574 dataset that included a large sample of carnivorans (Goswami 2006a). However, it underscores  
575 the flexibility of the model selection approach advocated here, in that many different proposed  
576 model structures can be simultaneously compared. The approach implemented in EMMLi, and  
577 its many possible future extensions, provides the ability to directly compare diverse hypotheses  
578 on the evolution of modularity and integration, which will become increasingly crucial as we  
579 drift further from well-established model systems. Further work along these lines will be crucial  
580 to identifying where shifts in modularity occur in the tree of life, and what the consequences of  
581 those shifts may be for the morphological evolution.

582

583 With respect to cranial modularity in macaques, the results from maximum likelihood analyses  
584 as implemented in EMMLi underscore two important biological points: 1) the model of two  
585 cranial modules based on a neurocranial and a facial module is not supported when compared  
586 with more complex six-module hypotheses, and 2) the 8-module structure, although biologically  
587 plausible, is not supported. This implies that while a functional model of a facial (masticatory)  
588 vs. neurocranial organization of the skull is too simplistic to describe phenotypic integration,  
589 there is also likely an upper limit to the complexity of cranial integration in the macaque system.  
590 In addition, because Model 7 is highly-supported in the infant, juvenile, and subadult data sets in  
591 addition to the two adult data sets, this pattern of morphological integration appears to be  
592 established very early in postnatal ontogeny in *Macaca*. This consistency through ontogeny  
593 confirms the previous analyses of this dataset (Goswami and Polly 2010), which suggested that,

594 although relative level of integration decreases through ontogeny, the overall pattern is  
595 conserved from infancy to adulthood.

596

## 597 CONCLUSIONS

598 The study of phenotypic modularity has seen rapid growth in recent years. New empirical studies  
599 are expanding the topic beyond model systems through development (Young 1959; Zelditch  
600 1988; Hallgrímsson et al. 2004; Zelditch et al. 2006; Goswami et al. 2009; Hallgrímsson et al.  
601 2009; Zelditch et al. 2009; Sears et al. 2012), across the tree of life (Armbruster et al. 2004;  
602 Young and Hallgrímsson 2005; Goswami 2006b, a; Goswami 2007; Bell et al. 2011; Bennett and  
603 Goswami 2011; Armbruster et al. 2014; Conner et al. 2014; Goswami et al. 2014), and even into  
604 the distant past (Goswami 2006a; Bell et al. 2011; Gerber and Hopkins 2011; Webster and  
605 Zelditch 2011a, b; Maxwell and Dececchi 2012; Meloro and Slater 2012; Gerber 2013; Goswami  
606 et al. 2015). Alongside this extension of taxonomic and temporal sampling, there has been an  
607 expansion of analytical tools for the evaluation of modularity and integration. Confirmatory  
608 approaches, in particular, have received much attention in recent years, with RV coefficient  
609 analysis in particular being heavily applied to the analysis of modularity. However, these  
610 approaches by and large are limited to the direct comparison of models with similar complexities  
611 and do not allow for mixed models, where some traits are highly integrated and others are not.  
612 The issues caused by these weaknesses in the existing approaches will become increasing  
613 problematic as workers diverge from well-studied models into new systems without well-  
614 established *a priori* hypotheses of trait relationships.

615

616 Here, we have presented a maximum likelihood and model selection approach to the evaluation  
617 of modularity, which can directly compare highly complex hypotheses of trait relationships,  
618 including comparisons of nested and non-nested models. We demonstrate this approach using  
619 multidimensional vector correlation matrices for a large dataset of macaque crania, confirming  
620 the results of previous analyses, but allowing, for the first time, robust discrimination of  
621 alternative models. Our results support a highly parameterized model of six cranial modules,  
622 with distinct levels of integration within modules, as well as between pairs of modules. This  
623 method is applicable to any metric of trait relationship, given the availability of an appropriate  
624 transformation, has appropriate Type I error rates, is robust to low sample sizes, and should be  
625 incorporated into the existing toolbox for the study of phenotypic modularity in diverse systems.

626

## 627 ACKNOWLEDGEMENTS

628 We thank Prabu Sivasubramaniam and Tim Lucas for development of the R code for EMMLi.  
629 Data were gathered at the Primate Research Institute in Inuyama, Japan, with funding provided  
630 by the Japanese Society for the Promotion of Science HOPE grant to AG. We thank M. Takai for  
631 his role in encouraging and facilitating the research trip to PRI. We thank D. Adams, P.D. Polly,  
632 E. Sherratt, C. Klingenberg, UCL's ADaPTiVE lab group, and the NHM-UCL-IC Palaeobiology  
633 journal club for relevant discussions and comments on this work. The development of this  
634 method was supported by a Leverhulme Trust research grant to AG (RPG 2013-124) and a  
635 European Research Council grant (ERC-STG-2014-637171) to AG.

636

## 637 REFERENCES

- 638 Ackermann, R. R. and J. M. Cheverud. 2000. Phenotypic covariance structure in tamarins (genus  
639 *Saguinus*): a comparison of variation patterns using matrix correlation and common  
640 principal components analysis. *American Journal of Physical Anthropology* 111:489-501.
- 641 Adams, D. C. 2016. Evaluating modularity in morphometric data: challenges with the RV  
642 coefficient and a new test measure. *Methods Ecol. Evol.* in press.
- 643 Adams, D. C. and R. N. Felice. 2014. Assessing trait covariation and morphological integration  
644 on phylogenies using evolutionary covariance matrices. *PLoS ONE* 9:e94335.
- 645 Akaike, H. 1973. Information theory as an extension of the maximum likelihood principle. Pp.  
646 267-281 in B. N. Petrov, and F. Csaki, eds. *Second International Symposium on*  
647 *Information Theory*. Akademiai Kiado, Budapest.
- 648 Armbruster, W. S., C. Pelabon, G. H. Bolstad, and T. F. Hansen. 2014. Integrated phenotypes:  
649 understanding trait covariation in plants and animals. *Phil Trans Roy Soc Lon B*  
650 369:20130245.
- 651 Armbruster, W. S., C. Pélabon, T. F. Hansen, and C. P. H. Mulder. 2004. Floral integration,  
652 modularity, and accuracy: distinguishing complex adaptations from genetic constraints.  
653 Pp. 23-49 in M. Pigliucci, and K. Preston, eds. *Phenotypic integration*. Oxford University  
654 Press, Oxford.
- 655 Bell, E., B. Andres, and A. Goswami. 2011. Limb integration and dissociation in flying  
656 vertebrates: a comparison of pterosaurs, birds, and bats. *J. Evol. Biol.* 24:286-2599.
- 657 Bennett, C. V. and A. Goswami. 2011. Does reproductive strategy drive limb integration in  
658 marsupials and monotremes? *Mammalian Biology* 76:79-83.
- 659 Bookstein, F. L. and P. Mitteroecker. 2014. Comparing covariance matrices by relative  
660 eigenanalysis, with applications to organismal biology. *Evol. Biol.* 41:336-350.
- 661 Burnham, K. P. and D. R. Anderson. 2002. *Model Selection and Multimodel Inference: A*  
662 *Practical Information-Theoretic Approach*. Springer, New York.
- 663 Burnham, K. P. and D. R. Anderson. 2004. Multimodel inference: Understanding AIC and BIC  
664 in model selection. *Sociological Methods and Research* 33:261-304.
- 665 Cheverud, J. M. 1982. Phenotypic, Genetic, and Environmental Morphological Integration in the  
666 Cranium. *Evolution* 36:499-516.
- 667 Cheverud, J. M. 1989. A comparative analysis of morphological variation patterns in the  
668 Papionines. *Evolution* 43:1737-1747.
- 669 Cheverud, J. M. 1995a. Morphological integration in the saddle-back tamarin (*Saguinus*  
670 *fuscicollis*) cranium. *Am. Nat.* 145:63-89.
- 671 Cheverud, J. M. 1995b. Morphological integration in the saddle-back tamarin (*Saguinus*  
672 *fuscicollis*) cranium. *Am. Nat.* 145:63-89.
- 673 Cheverud, J. M. 1996. Developmental integration and the evolution of pleiotropy. *Am. Zool.*  
674 36:44-50.
- 675 Conner, J. K., I. A. Cooper, R. J. L. Rosa, S. G. Perez, and A. M. Royer. 2014. Patterns of  
676 phenotypic correlations among morphological traits in plants and animals. *Phil Trans Roy*  
677 *Soc Lon B* 369:20130246.
- 678 De Leeuw, J. 1983. Models and methods for the analysis of correlation coefficients. *Journal of*  
679 *Econometrics* 22:113-137.
- 680 Drake, A. G. and C. P. Klingenberg. 2010. Large-scale diversification of skull shape in domestic  
681 dogs: disparity and modularity. *Am. Nat.* 175:289-301.



- 682 Edwards, A. W. F. 1992. Likelihood: Expanded Edition. The Johns Hopkins University Press,  
683 Baltimore.
- 684 Feldman, G., A. Hayes, S. Kumar, J. Greeson, and J.-P. Laurenceau. 2007. Mindfulness and  
685 emotion regulation: The development and initial validation of the Cognitive and  
686 Affective Mindfulness Scale-Revised (CAMS-R). *Journal of Psychopathology and*  
687 *Behavioral Assessment* 29:177-190.
- 688 Fruciano, C., P. Franchini, and A. Meyer. 2013. Resampling-based approaches to study variation  
689 in morphological modularity. *PLoS ONE* 8:e69376.
- 690 Gerber, S. 2013. On the relationship between the macroevolutionary trajectories of  
691 morphological integration and morphological disparity. *PLoS ONE* 8:e63913.
- 692 Gerber, S. and M. J. Hopkins. 2011. Mosaic heterochrony and evolutionary modularity: the  
693 trilobite genus *Zacanthopsis* as a case study. *Evolution* 65:3241-3252.
- 694 Goswami, A. 2006a. Cranial modularity shifts during mammalian evolution. *Am. Nat.* 168:270-  
695 280.
- 696 Goswami, A. 2006b. Morphological integration in the carnivoran skull. *Evolution* 60:169-183.
- 697 Goswami, A. 2007. Phylogeny, diet, and cranial integration in australodelphian marsupials.  
698 *PLoS One* 2:e995.
- 699 Goswami, A., W. J. Binder, J. A. Meachen, and F. R. O'Keefe. 2015. The fossil record of  
700 phenotypic integration and modularity: a deep-time perspective on developmental and  
701 evolutionary dynamics. *Proc. Natl. Acad. Sci. U. S. A.* 112:4891-4896.
- 702 Goswami, A. and P. D. Polly. 2010. Methods for studying morphological integration and  
703 modularity. Pp. 213-243 in J. Alroy, and E. G. Hunt, eds. *Quantitative Methods in*  
704 *Paleobiology*. Paleontological Society Special Publications.
- 705 Goswami, A., J. B. Smaers, C. Soligo, and P. D. Polly. 2014. The macroevolutionary  
706 consequences of phenotypic integration: from development to deep time. *Phil Trans Roy*  
707 *Soc Lon B* 369:20130254.
- 708 Goswami, A., V. Weisbecker, and M. R. Sanchez-Villagra. 2009. Developmental Modularity and  
709 the Marsupial-Placental Dichotomy. *J. Exp. Zool. Part B* 312B:186-195.
- 710 Hallgrímsson, B., H. Jamniczky, N. M. Young, C. Rolian, T. E. Parsons, J. C. Boughner, and R.  
711 S. Marcucio. 2009. Deciphering the palimpsest: studying the relationship between  
712 morphological integration and phenotypic covariation. *Evol. Biol.* 36:355-376.
- 713 Hallgrímsson, B., K. Willmore, C. Dorval, and D. M. L. Cooper. 2004. Craniofacial variability  
714 and modularity in macaques and mice. *J. Exp. Zool. Part B* 302B:207-225.
- 715 Hurvich, C. M. and C.-L. Tsai. 1989. Regression and time series model selection in small  
716 samples. *Biometrika* 76:297-307.
- 717 Klingenberg, C. P. 2008. Morphological integration and developmental modularity. *Annual*  
718 *Review of Ecology, Evolution, and Systematics* 39:115-132.
- 719 Klingenberg, C. P. 2009. Morphometric integration and modularity in configurations of  
720 landmarks: tools for evaluating a prior hypotheses. *Evol. Dev.* 11:405-421.
- 721 Klingenberg, C. P. 2013. Cranial integration and modularity: insights into evolution and  
722 development from morphometric data. *Hystrix* 24:43-58.
- 723 Klingenberg, C. P. 2014. Studying morphological integration and modularity at multiple levels:  
724 concepts and analysis. *Phil Trans Roy Soc Lon B* 369:in press.
- 725 Klingenberg, C. P. and J. Marugan-Lobon. 2013. Evolutionary covariation in geometric  
726 morphometric data: analyzing integration, modularity and allometry in a phylogenetic  
727 context. *Syst. Biol.* 62:591-610.

- 728 LeBel, E. P. and B. Gawronski. 2009. How to find what's in a name: Scrutinizing the optimality  
729 of five scoring algorithms for the name-letter task. *European Journal of Personality*  
730 23:85-106.
- 731 Marquez, E. J. 2008. A statistical framework for testing modularity in multidimensional data.  
732 *Evolution* 62:2688-2708.
- 733 Marroig, G. and J. M. Cheverud. 2001. A comparison of phenotypic variation and covariation  
734 patterns and the role of phylogeny, ecology, and ontogeny during cranial evolution of  
735 New World monkeys. *Evolution* 55:2576-2600.
- 736 Marroig, G., L. Shirai, A. Porto, F. B. de Oliveira, and V. De Conto. 2009. The evolution of  
737 modularity in the mammalian skull II: evolutionary consequences. *Evol. Biol.* 36:136-  
738 148.
- 739 Maxwell, E. E. and T. A. Dececchi. 2012. Ontogenetic and stratigraphic influence on observed  
740 phenotypic integration in the limb skeleton of a fossil tetrapod. *Paleobiology* 39:123-134.
- 741 Meloro, C. and G. J. Slater. 2012. Covariation in the skull modules of cats: the challenge of  
742 growing saber-like canines. *J. Vert. Paleontol.* 32:677-685.
- 743 Olson, E. C. and R. L. Miller. 1951. A mathematical model applied to the evolution of species.  
744 *Evolution* 5:325-338.
- 745 Olson, E. C. and R. L. Miller. 1958. *Morphological Integration*. University of Chicago Press,  
746 Chicago
- 747 Pavlicev, M., J. M. Cheverud, and G. P. Wagner. 2009. Measuring morphological integration  
748 using eigenvalue variance. *Evol. Biol.* 36:157-170.
- 749 Porto, A., F. B. de Oliveira, L. Shirai, V. De Conto, and G. Marroig. 2009. The evolution of  
750 modularity in the mammalian skull I: morphological integration patterns and magnitudes.  
751 *Evol. Biol.* 36:118-135.
- 752 Rohlf, F. J. and M. Corti. 2000. Use of two-block partial least-squares to study covariation in  
753 shape. *Syst. Biol.* 49:740-753.
- 754 Royall, R. M. 1997. *Statistical Evidence: A Likelihood Paradigm*. Chapman and Hall, New  
755 York.
- 756 Sears, K. E., C. Doroba, X. Cao, D. Xie, and S. Zhong. 2012. Molecular determinants of  
757 marsupial integration and constraint in R. J. Asher, and J. Mueller, eds. *From clone to*  
758 *bone: the synergy of morphological and molecular tools in palaeobiology*. Cambridge  
759 University Press, Cambridge.
- 760 Sokal, R. R. and F. J. Rohlf. 1995. *Biometry*. W. H. Freeman, New York.
- 761 Steiger, J. H. 1980a. Testing pattern hypotheses on correlation matrices: alternative statistics and  
762 some empirical results. *Multivariate Behavioral Research* 15:335-352.
- 763 Steiger, J. H. 1980b. Tests for comparing elements of a correlation matrix. *Psychological*  
764 *Bulletin* 87:245-251.
- 765 Wager, T. D., D. J. Scott, and J.-K. Zubieta. 2007. Placebo effects on human  $\mu$ -opioid activity  
766 during pain. *Proceedings of the National Academy of Sciences* 104:11056-11061.
- 767 Wagner, P. J. 2000. Likelihood tests of hypothesized durations: determining and accommodating  
768 biasing factors. *Paleobiology* 26:431-449.
- 769 Webster, M. and M. L. Zelditch. 2011a. Evolutionary lability of integration in Cambrian  
770 ptychoparioid trilobites. *Evol. Biol.* 38:144-162.
- 771 Webster, M. and M. L. Zelditch. 2011b. Modularity of a Cambrian ptychoparioid trilobite  
772 cranium. *Evol. Dev.* 13:96-109.

- 773 Young, N. M. and B. Hallgrímsson. 2005. Serial homology and the evolution of mammalian  
774 limb covariation structure. *Evolution* 59:2691-2704.
- 775 Young, R. W. 1959. The influence of cranial contents on postnatal growth of the skull in the rat.  
776 *American Journal of Anatomy* 105:383-415.
- 777 Zelditch, M. L. 1988. Ontogenetic variation in patterns of phenotypic integration in the  
778 laboratory rat. *Evolution* 42:28-41.
- 779 Zelditch, M. L., J. G. Mezey, H. D. Sheets, B. L. Lundrigan, and J. T. Garland. 2006.  
780 Developmental regulation of skull morphology II: Ontogenetic dynamics of covariance.  
781 *Evol. Biol.* 8:46-60.
- 782 Zelditch, M. L., A. R. Wood, and D. L. Swiderski. 2009. Building developmental integration into  
783 functional systems: function-induced integration of mandibular shape. *Evol. Biol.* 36:71-  
784 87.
- 785
- 786

For Peer Review Only

## 787 FIGURE CAPTIONS

788 Figure 1. Schematic depiction of three alternative partitions of the macaque cranium. A) No  
789 modularity, with similar levels of correlation among all landmarks. B) Two modules,  
790 corresponding to facial and neurocranial regions. C) Six modules, corresponding approximately  
791 to Cheverud's model (1982). Colored circles indicate module associations. Solid lines indicate  
792 within-module correlations. Dotted lines indicate between-module correlations.

793

794 Figure 2. Schematic depiction of the four alternative parameterizations of a single six-module  
795 model structure. A) Basic structure of landmark associations in six modules, indicated by  
796 colours. The six modules may have either similar (B) or different (C) magnitudes of within-  
797 module correlations. The intermodule correlations may also be similar (D and F) or different (E  
798 and G) among all pairs of modules. Each distinct estimated value of  $\rho$  is counted as a parameter,  
799 along with one additional parameter for estimated variance. Solid lines indicate within-module  
800 correlations. Dashed lines indicate between-module correlations. Line colours indicate similar or  
801 different estimated values for  $\rho$  (e.g., in B, the black lines indicate that all of the six modules  
802 have the same estimated within-module correlation).

803

804 Figure 3. Results of simulations demonstrating accuracy in model selection for different model  
805 structures (no modularity, two modules, or six modules), complexity (similar or different within-  
806 module correlations), and magnitudes of within-module correlations, modelled with varying  
807 standard deviations of A)  $\sigma = 0.01$  or B)  $\sigma = 0.05$ . Stacked bars show percentage of simulations

808 identifying: the correct model (green), an alternative parameterization of the same model  
809 structure, i.e., a related model, with posterior probability  $< 0.50$  (dark blue), a related model with  
810 posterior probability  $> 0.50$  (light blue), an unrelated model with posterior probability  $< 0.50$   
811 (pink), or an unrelated model with posterior probability  $> 0.50$  (red). Simulated mean within-  
812 module correlations, or all correlations for no modularity models, are indicated on the x-axis.  
813 100 simulations were run for each model, resulting in a total of 4200 simulations. Results show  
814 that this method is highly accurate at identifying the correct model structure, except where higher  
815 standard deviations are combined with extremely high correlations and simple model structures  
816 (no modularity, in particular).

817

## TABLES

**Table 1: Model descriptions and parameterizations for the 31 model structures explored in this study. Base models structures follow the allocation of landmark variables in Table S1. Model parameters are a sum of the number of estimated correlations within modules and across modules, plus one (for the estimate of the variance of the population correlation).**

Model ID	Base Model Structure	# Modules	Model description	# Parameters
1	No Modules	0	1 $\rho$ for all correlations	2
2	Neurocranial/Facial model	2	1 within module $\rho$ for both modules, 1 between-module $\rho$	3
3	Neurocranial/Facial model	2	2 within-module $\rho$ 's and 1 between-module $\rho$	4
4	Cheverud model	6	1 within-module $\rho$ and 1 between-module $\rho$	3
5	Cheverud model	6	Separate within-module $\rho$ 's and 1 between-module $\rho$	8
6	Cheverud model	6	1 within-module $\rho$ and separate between-module $\rho$ 's	17
7	Cheverud model	6	Separate within-module $\rho$ 's and separate between-module $\rho$ 's	22
8	Goswami model	6	1 within-module $\rho$ and 1 between-module $\rho$	3
9	Goswami model	6	Separate within-module $\rho$ 's and 1 between-module $\rho$	8
10	Goswami model	6	1 within-module $\rho$ and separate between-module $\rho$ 's	17
11	Goswami model	6	Separate within-module $\rho$ 's and separate between-module $\rho$ 's	22
12	Cheverud/Goswami	8	1 within-module $\rho$ and 1 between-module $\rho$	3

	combined model			
13	Cheverud/Goswami combined model	8	Separate within-module $\rho$ 's and 1 between-module $\rho$	10
14	Cheverud/Goswami combined model	8	1 within-module $\rho$ and separate between-module $\rho$ 's	30
15	Cheverud/Goswami combined model	8	Separate within-module $\rho$ 's and separate between-module $\rho$ 's	37
16	Tissue Origin model	3	1 within-module $\rho$ and 1 between-module $\rho$	3
17	Tissue Origin model	3	1 within-module $\rho$ and separate between-module $\rho$ 's	5
18	Tissue Origin model	3	Separate within-module $\rho$ and 1 between-module $\rho$ 's	5
19	Tissue Origin model	3	Separate within-module $\rho$ and separate between-module $\rho$ 's	7
20	Cheverud-based "monotreme" model	3	1 within-module $\rho$ (for modules 1, 2, and 6 only), 1 pooled between-module and unintegrated $\rho$	3
21	Cheverud-based "monotreme" model	3	1 within-module $\rho$ (for modules 1, 2, and 6 only), 1 between- module $\rho$ , and 1 unintegrated $\rho$	4
22	Cheverud-based "monotreme" model	3	Separate within-module $\rho$ 's (for modules 1, 2, and 6 only), 1 pooled between-module and unintegrated $\rho$	5
23	Cheverud-based	3	Separate within-module $\rho$ 's (for modules 1, 2, and 6 only), 1	6

	“monotreme” model		between-module $\rho$ , and 1 unintegrated $\rho$	
24	Cheverud-based	3	1 within-module $\rho$ (for modules 1, 2, and 6 only), separate	6
	“monotreme” model		between-module $\rho$ 's, and 1 unintegrated $\rho$	
25	Cheverud-based	3	Separate within-module $\rho$ 's (for modules 1, 2, and 6 only),	8
	“monotreme” model		separate between-module $\rho$ 's, and 1 unintegrated $\rho$	
26	Goswami-based	3	1 within-module $\rho$ (for modules 1, 2, and 6 only), 1 pooled	3
	“monotreme” model		between-module and unintegrated $\rho$	
27	Goswami-based	3	1 within-module $\rho$ (for modules 1, 2, and 6 only), 1 between-	4
	“monotreme” model		module $\rho$ , and 1 unintegrated $\rho$	
28	Goswami-based	3	Separate within-module $\rho$ 's (for modules 1, 2, and 6 only), 1	5
	“monotreme” model		pooled between-module and unintegrated $\rho$	
29	Goswami-based	3	Separate within-module $\rho$ 's (for modules 1, 2, and 6 only), 1	6
	“monotreme” model		between-module $\rho$ , and 1 unintegrated $\rho$	
30	Goswami-based	3	1 within-module $\rho$ (for modules 1, 2, and 6 only), separate	6
	“monotreme” model		between-module $\rho$ 's, and 1 unintegrated $\rho$	
31	Goswami-based	3	Separate within-module $\rho$ 's (for modules 1, 2, and 6 only),	8
	“monotreme” model		separate between-module $\rho$ 's, and 1 unintegrated $\rho$	



**Table 2: Results for the Sub-Adult (M2 erupted) data set (n=48) using congruence coefficients. Model parameters, raw log-likelihood fits for each tested model,  $AIC_c$  and  $\Delta AIC_c$  scores are provided. Model log-likelihoods and the model posterior probability are also shown. Sample size used to calculate  $AIC_c$  was 1830. See methods for details. Model ID's correspond to the numbering in Table 1. The optimal model in the set of evaluated models is highlighted in bold italics.**

Model ID	K	LogL	$AIC_c$	$\Delta AIC_c$	Model LogL	Model Post. Prob.
1	2	2078.86	-4153.72	916.21	1.11E-199	1.11E-199
2	3	2134.49	-4262.97	806.96	5.89E-176	5.89E-176
3	4	2147.54	-4287.06	782.88	1.00E-170	1.00E-170
4	3	2219.34	-4432.67	637.26	4.17E-139	4.17E-139
5	8	2380.83	-4745.58	324.35	3.69E-71	3.69E-71
6	17	2395.76	-4757.18	312.75	1.22E-68	1.22E-68
7	<b>22</b>	<b>2557.25</b>	<b>-5069.93</b>	<b>0.00</b>	<b>1.00</b>	<b>1.000</b>
8	3	2153.94	-4301.87	768.06	1.65E-167	1.65E-167
9	8	2226.56	-4437.03	632.90	3.69E-138	3.69E-138
10	17	2257.63	-4480.93	589.01	1.26E-128	1.26E-128
11	22	2330.25	-4615.93	454.00	2.60E-99	2.60E-99
12	3	2172.35	-4338.69	731.24	1.63E-159	1.63E-159
13	10	2246.04	-4471.95	597.98	1.41E-130	1.41E-130

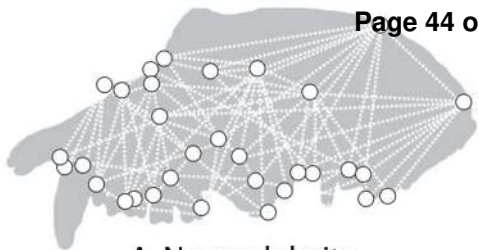
14	30	2417.44	-4773.85	296.09	5.07E-65	5.07E-65
15	37	2491.12	-4906.68	163.26	3.54E-36	3.54E-36
16	3	2079.47	-4152.93	917.00	7.50E-200	7.50E-200
17	5	2214.56	-4419.08	650.85	4.67E-142	4.67E-142
18	5	2109.73	-4209.43	860.51	1.39E-187	1.39E-187
19	7	2244.82	-4475.57	594.36	8.62E-130	8.62E-130
20	3	2262.47	-4518.93	551.01	2.24E-120	2.24E-120
21	4	2265.54	-4523.05	546.88	1.76E-119	1.76E-119
22	5	2324.39	-4638.75	431.18	2.34E-94	2.34E-94
23	6	2327.46	-4642.87	427.06	1.84E-93	1.84E-93
24	6	2286.11	-4560.17	509.76	2.03E-111	2.03E-111
25	8	2348.03	-4679.99	389.95	2.11E-85	2.11E-85
26	3	2181.12	-4356.23	713.70	1.05E-155	1.05E-155
27	4	2181.12	-4354.23	715.71	3.85E-156	3.85E-156
28	5	2204.15	-4398.27	671.66	1.42E-146	1.42E-146
29	6	2204.15	-4396.26	673.67	5.17E-147	5.17E-147
30	6	2195.90	-4379.76	690.18	1.35E-150	1.35E-150
31	8	2218.93	-4421.78	648.15	1.80E-141	1.80E-141

**Table 3: Optimal values of  $\rho$  within the six modules and for the 15 inter-module correlations estimated in Model 7 for each of the macaque data sets partitioned by ontogenetic stage.**

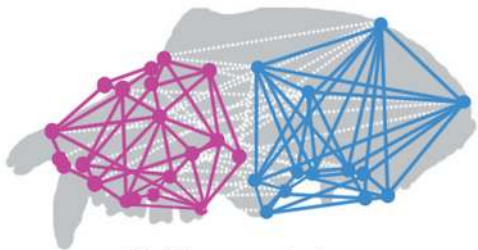
	Adult Females	Adult Males	Sub-Adult (M2 erupted)	Juvenile (M1 erupted)	Infant (Deciduous only)
<b>Module 1</b>	0.43	0.46	0.43	0.44	0.55
<b>Module 2</b>	0.77	0.77	0.81	0.76	0.67
<b>Module 3</b>	0.24	0.35	0.40	0.19	0.22
<b>Module 4</b>	0.15	0.18	0.14	0.16	0.15
<b>Module 5</b>	0.12	0.23	0.14	0.17	0.23
<b>Module 6</b>	0.28	0.29	0.30	0.30	0.28
<b>M1 to M2</b>	0.10	0.13	0.13	0.13	0.13
<b>M1 to M3</b>	0.22	0.29	0.35	0.21	0.31
<b>M1 to M4</b>	0.18	0.22	0.14	0.14	0.20
<b>M1 to M5</b>	0.21	0.21	0.22	0.22	0.29
<b>M1 to M6</b>	0.19	0.17	0.22	0.20	0.28
<b>M2 to M3</b>	0.13	0.22	0.08	0.08	0.12
<b>M2 to M4</b>	0.14	0.08	0.12	0.08	0.14
<b>M2 to M5</b>	0.07	0.09	0.10	0.13	0.10

<b>M2 to M6</b>	0.12	0.27	0.08	0.17	0.08
<b>M3 to M4</b>	0.11	0.15	0.11	0.11	0.13
<b>M3 to M5</b>	0.16	0.12	0.16	0.09	0.16
<b>M3 to M6</b>	0.11	0.12	0.15	0.10	0.14
<b>M4 to M5</b>	0.14	0.15	0.11	0.12	0.13
<b>M4 to M6</b>	0.13	0.12	0.11	0.11	0.11
<b>M5 to M6</b>	0.17	0.17	0.14	0.16	0.15

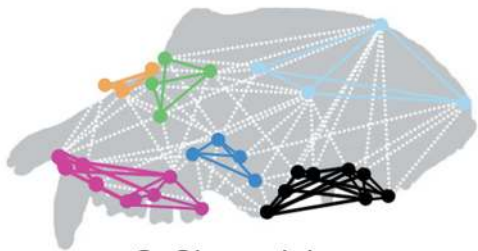
For Peer Review Only



A. No modularity



B. Two modules



C. Six modules

